Structural Engineering and Mechanics, *Vol. 58, No. 6 (2016) 967-988*
DOI: http://dx.doi.org/10.12989/sem.2016.58.6.967

Wind load effects and equivalent static wind loads of three-tower connected tall buildings based on wind tunnel tests

Shitang Ke[*1], Hao Wang[1a] and Yaojun Ge[2b]

[1]*Department of Civil Engineering, Nanjing University of Aeronautics and Astronautics, Yudao Road 29, Nanjing 210016,China*
[2]*State Key Laboratory for Disaster Reduction in Civil Engineering, Tongji University, Siping Road 1239, Shanghai 200092, China*

(Received March 24, 2015, Revised March 9, 2016, Accepted March 12, 2016)

Abstract. Due to the significant aerodynamic interference from sub-towers and surrounding tall buildings, the wind loads and dynamic responses on main tower of three-tower connected tall building typically change especially compared with those on the isolated single tall building. This paper addresses the wind load effects and equivalent static wind loads (ESWLs) of three-tower connected tall building based on measured synchronous surface pressures in a wind tunnel. The variations of the global shape coefficients and extremum wind loads of main tower structure with or without interference effect under different wind directions are studied, pointing out the deficiency of the traditional wind loads based on the load codes for the three-tower connected tall building. The ESWLs calculation method based on elastic restoring forces is proposed, which completely contains the quasi-static item, inertia item and the coupled effect between them. Then the wind-induced displacement and acceleration responses for main tower of three-tower connected tall building in the horizontal and torsional directions are investigated, subsequently the structural basal and floor ESWLs under different return periods, wind directions and damping ratios are studied. Finally, the action mechanism of interference effect on structural wind effects is investigated. Main conclusions can provide a sientific basis for the wind-resistant design of such three-tower connected tall building.

Keywords: three-tower connected tall building; wind tunnel test; equivalent static wind load; wind loads; wind effect; interference effect

1. Introduction

Historically, wind loads and wind-induced interference effect on tall buildings have always been a concern (Kareem 1981, Bailey and Kwok 1985, Khanduri *et al*. 1998), wind load is one of the control loads of multi-tower connected tall buildings, which is directly related to the structural safety and comfort. In addition, due to the significant aerodynamic interference from annex and surrounding tall buildings, the wind loads and wind-induced responses on main tower structure of multi-tower connected tall building typically change especially when compared with the wind

∗Corresponding author, Associate Professor, E-mail: keshitang@163.com
[a]Postgraduate, E-mail: wanghaonuaa@163.com
[b]Professor, E-mail: yaojunge@tongji.edu.cn

http://www.techno-press.org/?journal=sem&subpage=8 ISSN: 1225-4568 (Print), 1598-6217 (Online)

effects on isolated single strutures. The studies on wind loads and effects for two tall buildings or twin-tower connected tall building (Xie and Gu 2004, Lam *et al*. 2008, Zhao and Lam 2008, Li and Sumner 2009, Kim *et al*. 2011) have shown that the global shape coefficients and gust response factor (GRF) on main towers of twin-tower connected tall buildings are obviously amplified, and the typical wind effects and ESWLs are obviously different from that of isolate single tall buildings. Furthermore, the related researches (Lim *et al*. 2011, Tanaka *et al*. 2012, Song and Tse 2014, Liang *et al*. 2014, Tse and Song 2015, Song *et al*. 2016) show that the wind loads and wind-induced responses of linked building system are reduced in comparison with those of two independent towers without a link, attributing to the additional link stiffness as mobilizing the stiffness of an individual tower to resist the lateral wind loads. The flow interference occurs when three or more buildings are connected in close proximity, therefore, the interference effect should be taken into account in wind tunnel tests and numerical simulation for these tall buildings.

Wind loads on tall buildings can be quantified through syncharonous pressure measurements in wind tunnel tests, or by high frequency force balance (HFFB) measurements, or by simplified wind load codes. The HFFB measurements provide an estimate of the generalized forces of the fundamental modes of structural vibration, the wind load codes offer simplified and conservative ESWLs on isolated tall buildings with simple geometric configurations, while the synchronous pressure measurements can give a detail description of spatiotemporally varying wind loads (Zhou and Kareem 2001, Xie and Gu 2007). For tall buildings, the fundamental mode contribution dominates global building response such as the top displacement and base bending moment. However, higher modes may have noticeable contribution to some response such as the top acceleration and ESWLs, especially the complex geometric configurations or multi-tower connected tall buildings. The studies by Simiu (1976), Simiu and Scanlan (1996), Kareem and Zhou (2003) using analytical loading models demonstrated that the contributions from higher modes may reach to about 20% of the top acceleration. The ESWLs are adopted in the current design practice to represent the dynamic wind loads, the GRF approach proposed by Davenport (1967) has been widely used in design codes and standards worldwide for wind loads. This approach leads to ESWLs given by the mean wind loads multiplied by a GRF, often associated with the top displacement. However, studies have shown that GRF may vary widely for different response objectives, and the GRF approach falls short in providing physically meaningful ESWLs for the accrosswind load and torsional responses, which are typically characterized by zero mean wind responses. The advanced ESWLs modeling on tall buildings including background and resonant components has been addressed extensively in the literatures. However, the background component can be treated as a quasi-static load determined based on the load-response-correlation (LRC) approach (Kasperski 1992, Kasperski and Niemann 1992). The resonant load component follows the distribution of the inertial load and can be expressed in terms of modal inertial loads (Irwin 1998, Solari and Kareem 1998, Holmes 2002, Chen and Kareem 2005). Finally, the fluctuating wind-induced response and ESWLs are obtained by SRSS combination of background and resonant components, which ignores the higher modes contribution to resonant component and the coupling component between background and resonant response.

For that reason, this study addresses the wind load effects and ESWLs for main tower of three-tower connected tall building. First, the refined wind-induced responses and ESWLs calculating method based on wind-induced forces is proposed, which completely contains the quasi-static item, inertia item and the coupled effect between them. Then based on the measured synchronous surface pressures for the three-tower connected tall building and surrounding interference buildings in a wind tunnel, the global shape coefficients and extremum wind loads of

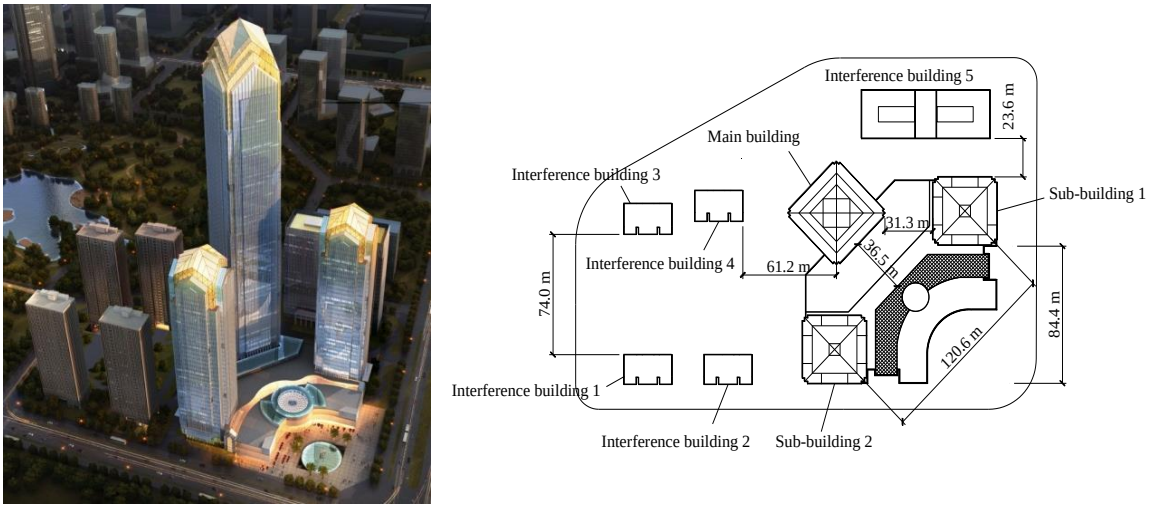

(a) architectural rendering (b) the layout plan with labels

Fig. 1 The buildings layout and labels of three-tower connected tall building with surrounding buildings

main tower structure with or without interference effect under different wind directions are studied in detail. Finally, the wind-induced displacement and acceleration responses, wind vibration coefficients, ESWLs and basal internal forces for main tower structure in the horizontal and torsional directions are investigated with different return periods and damping ratios. For the completeness, the action mechanism of interference effect for three-tower connected tall building is studied.

2. Wind tunnel experiment

The buildings layout and labels can be found in Fig. 1. The height of 63-floor main tower of three-tower connected tall building is 300 m, the height of sub-towers 1 and 2 is 156 m, the height of surrounding interference buildings is 105 m, and the height of surrounding buildings 1-4 is 103 m. Wind can cause severe damage to the structures because they are located in a hurricane-prone region in coastal area of East China.

The wind tunnel test was performed in the NH-2 Boundary Layer Wind Tunnel in Nanjing University of Aeronautics and Astronautics to obtain the pressure distribution on the main tower surface. The wind tunnel working section is 5.0 m wide and 4.2 m high. The geometrical scale ratio used was 1:300, and a total of 340 measuring taps were arranged in the four sides of the main tower. Fluctuating wind pressures at 330 Hz and 60 s were simultaneously measured at the 340 measuring taps on a rigid model of the main tower. The azimuth range of 0°-360° was taken, and the interval between angles was 10°. The 0° wind direction was defined as wind parallel to the horizontal force *X*-direction of the main tower structure. The detailed parameters and wind directions are shown in Fig. 2. Pressure taps were connected with a measurement system made of PVC tubing. Signals were modified using the transfer function of the tubing systems to avoid distortion of the dynamic pressures. Figs. 3 and 4 presents the photograph of the rigid models and measured points, where the three-tower connected tall building and surrounding interfering

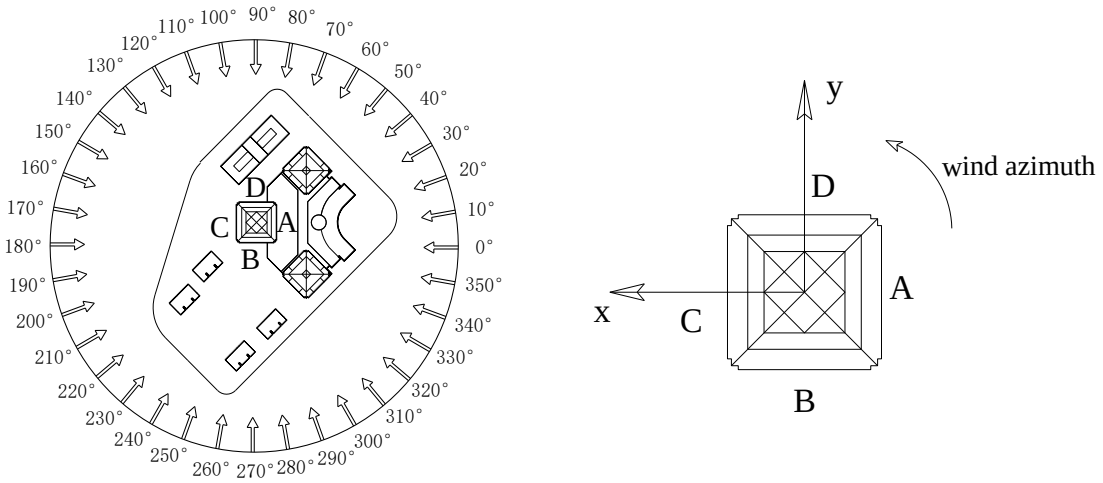

(a) Wind azimuth definition (b) The force analysis coordinate

Fig. 2 Wind tunnel test of wind azimuth and coordinate schematic diagram

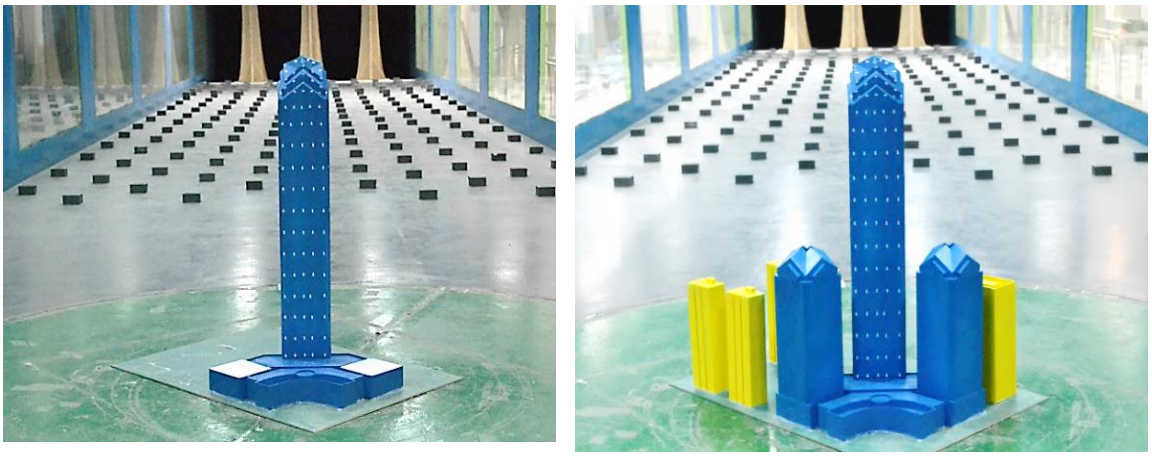

(a) The single main tower structure (b) Three-tower conjoined building with surroundings buildings

Fig. 3 Model arrangement plan in wind tunnel pressure test

buildings are presented.

The wind field of terrain category *B*, in accordance with the Chinese Code (GB5009-2012 2012), was simulated with a standard spire-roughness arrangement on the wind tunnel floor. The exponent of the mean wind speed profile for terrain category *B* was 0.15. The reference wind speed height is 1.0 m in wind tunnel.

Wind pressure obtained from the pitot tube was used to calculate the non-dimensional pressure coefficients. The non-dimensional net pressure coefficient was determined by

$$C_{pi,\theta} = \frac{P_{i,\theta} - \overline{P}_s}{\overline{P}_{t,h} - \overline{P}_s} = \frac{P_{i,\theta} - \overline{P}_s}{0.5\rho\overline{V}_h^2} \tag{1}$$

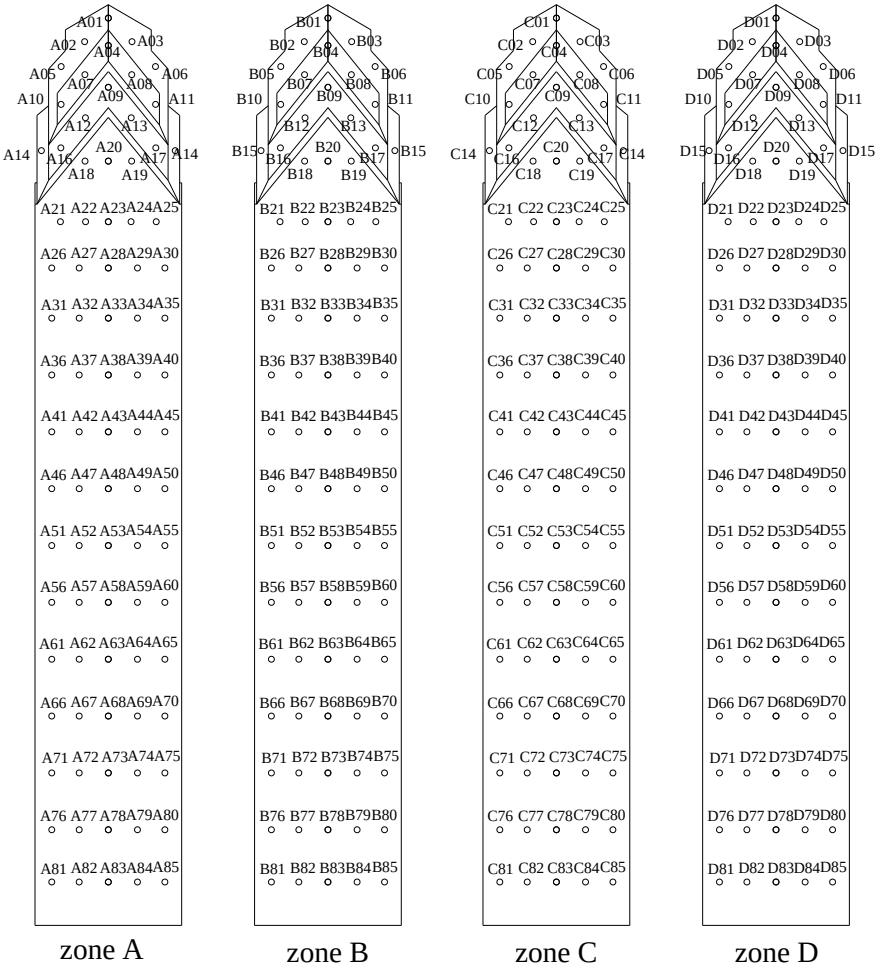

Fig.4 Main tower zone distribution and measuring point arrangement plan

where $C_{pi,\theta}$ is the pressure coefficient at the ith measuring point in wind direction θ, $P_{i,\theta}$ is the pressure at the ith measuring point, $\overline{P}_s$ and $\overline{P}_{t,h}$ are the static pressure and total pressure of the pitot tube at reference points in the wind tunnel, respectively. $\overline{V}_h$ is the wind velocity at reference point.

Shape coefficient is the ratio of the actual stress on the surface and the wind flow pressure in the same height. The shape coefficient can be obtained through pressure coefficient as follows

$$\mu_{i,\theta} = \overline{C}_{pi,\theta} / \left(Z_i / h \right)^{2\alpha} \tag{2}$$

where $\mu_{i,\theta}$ is the shape coefficient at the ith measuring point in wind direction θ, Z_i is the height of ith measuring point, α is the exponent of the mean wind speed profile for terrain category B.

The extreme values of wind pressure coefficients are calculated as follows

$$C_{pi,\theta,\max} = C_{pi,\theta,mean} + gC_{pi,\theta,ms} \tag{3}$$

$$C_{pi,\theta,\min} = C_{pi,\theta,mean} - gC_{pi,\theta,ms} \tag{3}$$

where $C_{pi,\theta,\max}$, $C_{pi,\theta,\min}$, $C_{pi,\theta,mean}$, $C_{pi,\theta,ms}$ are maximum, minimum, mean and RMS values of pressure coefficients at ith measuring point in wind direction θ. g is the peak factor.

The global shape coefficient is calculated as follows

$$\mu_s = \left(\sum_i \mu_{si} A_i \right) / A \tag{4}$$

where μ_{si} is the shape coefficient at the ith measuring poin, A_i is the corresponding area of ith measuring point, A is the projected area of horizontal directions.

3. Calculating method of wind-induced response and ESWLs

3.1 Refined expressions of total coupled method

The equation governing the motion of a structure under wind loads can be written in a matrix style as

$$M\ddot{y} + C\dot{y} + Ky = Tp(t) \tag{5}$$

where $\boldsymbol{p}$ means external stochastic wind load vector; $\boldsymbol{M}$, $\boldsymbol{C}$, $\boldsymbol{K}$ means Mass, damping and stiffness matrix, respectively, $\ddot{y}(t)$, $\dot{y}(t)$ and $y(t)$ are the joint acceleration, velocity and displacement vectors, $\boldsymbol{T}$ means Force indicating matrix (m-by-n matrix) composed of zeros and ones, which is used to match the dimension number of nodes number and external load vector.

Using the modal coordinates, the dynamic displacement can be represented as

$$y(t) = \Phi q(t) = \sum_{i=1}^{n} \phi_i q_i(t) \approx \sum_{i=1}^{m} \phi_i q_i(t) + \sum_{i=m+1}^{n} \phi_i q_i(t) = y_d + y_s \tag{6}$$

Where n is the freedom degree number of all nodes, m is the number where the resonant contribution need be considered, $\boldsymbol{y_d}$=the response considering the background and resonant contribution of former m modes, $\boldsymbol{y_s}$=the response only considering quasi-static contribution of remaining modes, $\boldsymbol{q}$=generalized displacement vector, and $\boldsymbol{\Phi}$=Matrix of modes of vibration.

The total response is $\boldsymbol{K}^{-1}\boldsymbol{P}(t)$ under the wind loads vector $\boldsymbol{P}(t)$, unfolded as

$$K^{-1}p(t) = \sum_{i=1}^{n} F_i p(t) = \sum_{i=1}^{m} F_i p(t) + \sum_{i=m+1}^{n} F_i p(t) \tag{7}$$

where $\boldsymbol{F_i}$=flexibility matrix of the i_{th} mode, given by

$$F_i = \frac{\phi_i \phi_i^T}{\phi_i^T K \phi_i} \tag{8}$$

Then the static response $\boldsymbol{y_s}$ only considering quasi-static contribution of remaining modes is expressed by

$$y_s = \sum_{i=m+1}^{n} F_i p(t) = K^{-1} p(t) - \sum_{i=1}^{m} F_i p(t) \tag{9}$$

Combine Eq. (6) and Eq. (9), ***y(t)*** is expressed as

$$y(t) = y_d + y_s = \sum_{i=1}^{m} \phi_i q_i(t) + K^{-1} p(t) - \sum_{i=1}^{m} F_i p(t) = \sum_{i=1}^{m} (\phi_i q_i(t) - F_i p(t)) + K^{-1} p(t) \tag{10}$$

Accordingly, the background and resonant responses are given by

$$y(t)_b = K^{-1} p(t) \tag{11}$$

$$y(t)_r = \sum_{i=1}^{m} (\phi_i q_i(t) - F_i p(t)) \tag{12}$$

And $\boldsymbol{\sigma_t}$=root-mean-square (RMS) value of ***y(t)***, is expressed by

$$\sigma_t = \sqrt{\sigma_r^2 + \sigma_b^2 + 2\rho_{r,b}\sigma_r\sigma_b} = \sqrt{\sigma_r^2 + \sigma_b^2 + \sigma_c^2} \tag{13}$$

where $\boldsymbol{\sigma_b}$, $\boldsymbol{\sigma_r}$, $\boldsymbol{\sigma_c}$ are the response component vector of background, resonant and coupled term, respectively, and $\rho_{r,b}$ is correlation coefficient between background and resonant component (Huang and Chen 2007).

It can be found in Eq. (13) that fluctuating wind-induced responses should include background, resonant and coupled component. However, the tri-component method based on SRSS combination cannot consider the coupled component, which is acceptable for the small value of $\rho_{r,b}$, but widely different for some throng coupled structures. Due to the complex calculation process of $\rho_{r,b}$, the approach of solving coupled component based on covariance matrix of coupled restoring force in this paper is presented.

3.2 Covariance matrix of resonant (background, coupled and generalized) Elastic restoring force

The generalized displacement response of the i_{th} mode only containing resonant component from (12) is

$$q_{r,i}(t) = q_i(t) - \frac{\phi_i^T p(t)}{\phi_i^T K \phi_i} = q_i(t) - \frac{F_i(t)}{K_i} \tag{14}$$

Accordingly, the cross-power spectrum of generalized resonant displacement between the i_{th} mode and the j_{th} mode is expressed as

$$S_{q_{r,i},q_{r,j}}(\omega) = \int_{-\infty}^{\infty} R_{q_{r,i},q_{r,j}}(\tau) e^{-i2\pi\omega\tau} d\tau = (H_i^*(\omega) - \frac{1}{K_i})(H_j(\omega) - \frac{1}{K_j}) S_{F_i,F_j}(\omega) = H_{r,i}^*(\omega) H_{r,j}(\omega) S_{F_i,F_j}(\omega) \tag{15}$$

where $\boldsymbol{H_{r,i}}=\boldsymbol{H_i}(\omega)$-$1/\boldsymbol{K_i}$, is the resonant transfer function of the i_{th} mode. $\boldsymbol{K_i}$=stiffness matrix of the i_{th} mode, which can be expressed as

$$K_i = (\phi_i^T K \phi_i) / (\phi_i \phi_i^T) \tag{16}$$

The covariance of generalized resonant response is given by

$$C_{qq,r} = \int_{-\infty}^{\infty} H_r^* S_{FF} H_r d\omega = \int_{-\infty}^{\infty} H_r^* \Phi^T T D S_{AA} D^T T^T \Phi H_r d\omega \tag{17}$$

where $\boldsymbol{A}$, $\boldsymbol{D}$=time coordinate vector and proper modes matrix with POD method (Katsumura *et al*. 2007). Because the dimension number of $\boldsymbol{p}(t)$ is very large, so the POD method is used to reduce the dimension number of $\boldsymbol{p}(t)$ and save computing time.

And accordingly, the resonant elastic restoring force vector can be represented as

$$P_{eqq,r} = Ky(t)_r = K\Phi q(t)_r = M\Phi\Lambda q(t)_r \tag{18}$$

The cross-covariance matrix $\boldsymbol{C_{pp,r}}$ of $\boldsymbol{P_{eqq,r}}$ is expressed as

$$C_{pp,r} = \overline{P_{eqq,r}P_{eqq,r}} = M\Phi\Lambda C_{qq,r}\Lambda^T\Phi^T M^T \tag{19}$$

It can be easily seen that the accuracy of $\boldsymbol{P}_{eqq,r}$ is determined by the number of calculating mode and dynamic characteristic of structure, and $\boldsymbol{C}_{pp,t}$=the covariance matrix of total fluctuating elastic restoring force, can be obtained with Eq. (19) as long as resonant transfer function $\boldsymbol{H_r}$ is replaced by generalized transfer function $\boldsymbol{H}$. In this paper, in order to calculate coupled component, the covariance matrix of coupled elastic restoring force $\boldsymbol{C}_{pp,c}$ is defined, which is given by

$$C_{pp,c} = C_{pp,t} - (C_{pp,b} + C_{pp,r}) \tag{20}$$

3.3 Unified theory model

As is generally known, the background component can be obtained from the covariance matrix of external wind load $\{p(t)\}$ through the LRC approach (Kasperski and Niemann 1992). It is significant that the resonant and cross terms can be regarded as quasi-static response under inertial load excitation and coupling elastic restoring force, which is firstly proposed in this paper. Then, the resonant and cross response can be obtained using the LRC approach. Thus, Eq. (13) can be expressed by

$$[I]\left[C_{pp}\right]_t[I]^T = [I]\left[C_{pp}\right]_b[I]^T + [I]\left[C_{pp}\right]_r[I]^T + [I]\left[C_{pp}\right]_c[I]^T \tag{21}$$

where $[C_{pp}]_t$=covariance matrix of total fluctuating elastic restoring force; $[C_{pp}]_b$=covariance matrix of external wind load $\{p(t)\}$; $[C_{pp}]_r$=covariance matrix of resonant elastic restoring force; $[C_{pp}]_c$=covariance matrix of coupling elastic restoring force; and I=influence coefficient matrix.

The advantage of the LRC method is that the coupling effect of all modes is considered through the covariance matrix, which is utilized by the unified theory modal to calculate the resonant component and cross term exactly. Furthermore, the theory foundation of ESWLs for cross term response are presented by the LRC method based on the covariance matrix of coupling elastic restoring force $[C_{pp}]_c$.

3.4 Wind-induced response of resonant, background and cross term

Based on the unified theory model, the resonant and coupled response can be obtained using LRC method, take the resonant component as the example, an arbitrary dynamic response of interest $\boldsymbol{r(t)}$ is given by

$$r(t)_r = IP_{eqqr} = IM\Phi\Lambda q(t)_r \tag{22}$$

And the covariance matrix of resonant response ***r(t)*** is expressed as

$$C_{rr,r} = \overline{r(t)_r\, r(t)_r} = IC_{pp,r}I^T = IM\Phi\Lambda C_{qq,r}\Lambda^T\Phi^T M^T I^T \tag{23}$$

where $\boldsymbol{\Lambda}$ = diag($\omega^2_{1,\ \cdots\ ,}\omega^2_{\mathrm{m}}$). The RMS value vector of resonant response is given by

$$\boldsymbol{\sigma}_{R,r} = \sqrt{diag\left(C_{rr,r}\right)} \tag{24}$$

where diag(·)=the column vector of diagonal elements of $\boldsymbol{C}_{rr,r}$. The resonant ESWLs of response R_i is

$$\boldsymbol{P}_{er,i} = \left[C_{pp}\right]_{\boldsymbol{r}} \boldsymbol{I}_i^T \Big/ \sigma_{Ri,r} \tag{25}$$

where I_i is the row vector of influence coefficient matrix I.

Accordingly, if the $\boldsymbol{C}_{rr,r}$ is replaced with $\boldsymbol{C}_{rr,b}$, $\boldsymbol{C}_{rr,c}$, $\boldsymbol{C}_{rr,t}$, we can obtain background, coupled and total fluctuating wind-induced response using the same thought.

3.5 Combination of consistent coupled method

The total fluctuating response can be given by

$$\sigma_t = \sqrt{\sigma_r^2 + \sigma_b^2 + sign(diag(C_{rr,c}))\sigma_c^2} \tag{26}$$

Accordingly, the totally response of the tower is then given by

$$R_a = \bar{R} + g \times \sqrt{\sigma_r^2 + \sigma_b^2 + sign(diag(C_{rr,c}))\sigma_c^2} \tag{27}$$

where $\boldsymbol{R_a}$ is the total wind induced response which contains the mean term, background term, resonant term and cross term. g is the peak factor, set as 2.5 here.

Accordingly, the equivalent static peak load distribution is given by

$$P_e = \bar{P} + sign(\bar{R}) \times (W_B P_{eb} + W_R P_{er} + W_C P_{ec}) \tag{28}$$

where W_B, W_R and W_C are weighting factor of P_{eb}, weighting factor of P_{er} and weighting factor of P_{ec}, respectively, and are expressed by

$$W_R = \frac{\sigma_r}{\sigma_t}; \qquad W_B = \frac{\sigma_b}{\sigma_t}; \qquad W_C = \frac{\sigma_c}{\sigma_t} \tag{29}$$

3.6 Wind-induced acceleration responses

The building acceleration is of interest for the building habitability design, which can be determined through model analysis in either time or frequency domain. When the frequency domain approach is employed, the RMS value of the background and resonant components of the nth generalized acceleration are determined as

$$\sigma_{\ddot{q}nb} = \frac{1}{K_n}\sqrt{\int_0^\infty \left(2\pi f\right)^4 S_{qn} df} \tag{30}$$

$$\sigma_{\ddot{q}nr} = \omega_n^2 \sigma_{qnr} = \frac{1}{M_n} \sqrt{\int_0^\infty \frac{\pi f_n}{4\xi n} S_{qn}(f_n)} \tag{31}$$

where K_n, M_n are the generalized stiffness and mass, respectively. S_{qn} is the power spectral density function of the generalized force.

The background acceleration is generally negligibly small as compared to the resonant component. When only the resonant component is considered, the RMS value of the acceleration at the jth floor level is given by

$$\sigma_{aj} = \sum_{j=1}^{n} \sum_{k=1}^{n} \phi_j \phi_k \sigma_{\ddot{q}_{jr}} \sigma_{\ddot{q}_{kr}} \rho_{jkr} \tag{32}$$

where ρ_{jkr} (Huang and Chen 2007) is the correlation coefficient between the *j*th and *k*th resonant modal responses, which depends on not only the frequency ratio and damping ratios, but also the coherence of the generalized forces.

4. Results and discussion

4.1 Computing parameters

The wind and structural parameters for dynamic computation are as follows: (1) terrain category is *B*; (2) 10 minute averaged wind speed at 10m height for 50 years return period is 33.46 m/s, 10 minute averaged wind speed at 10m height for 10 years return period is 28.28 m/s; (3) structural damping ratio for wind-induced response is 2.5% and 2.0%, structural damping ratio for comfort performance is 1.5%; (4) the number of resonant mode participating in vibration is 50, and the all modes are considered in background response; (5) peak factor for extreme wind pressure and response is set as 2.5.

Table 1 The natural frequencies of front 10 mode shapes for the main tower

Modal number	Frequency/Hz	Modal mass participation factor/ %		
		X-axis translation	*Y*-axis translation	*Z*-axis torsion
1	0.16	0.12	64.95	0.00
2	0.17	63.72	0.13	0.00
3	0.48	0.00	0.00	78.97
4	0.68	0.00	18.65	0.00
5	0.73	18.82	0.00	0.00
6	1.33	0.01	0.00	10.28
7	1.47	0.00	5.40	0.00
8	1.67	6.15	0.00	0.04
9	2.17	0.09	0.00	3.13
10	2.44	0.00	3.04	0.00

4.2 Mode analysis

The structural frequencies and modal mass participation factors of front 10 mode shapes are shown in Table 1, the first natural frequency is 0.16 Hz, and the front 10 mode shapes range from 0.16 to 2.44 Hz. The natural frequencies are found to be very small and fairly close to one another. The modal mass participation factor from the second mode in *X*-axis translation is the maximum 63.72%, and in *Y*-axis translation is 64.95% from first mode, and in *Z*-axis torsion is 78.97% from third mode. This is a very important to consider the modal coupled effects between the resonant modes and background modes when analyzing the wind-induced dynamic responses.

4.3 Wind loads characteristics

Extreme wind pressure is the important parameter of wind-resistant design for tall buildings. Figs. 5-7 respectively present the surface extreme wind pressure coefficients under single condition, interference condition and enveloping condition with different wind directions. It can be found from figures:

(1) The maximum wind pressure coefficients under single and interference conditions with different wind directions are mostly located in the upper area of surface *B*, and the extreme values of wind pressure coefficients in surface *B* are obviously bigger than those in other surfaces. The maximum wind pressure coefficients under single condition are generally greater than those under interference condition.

(2) Different with the maximum wind pressure coefficients, the minimum wind pressure coefficients in four surfaces of main tower structure under single and interference conditions

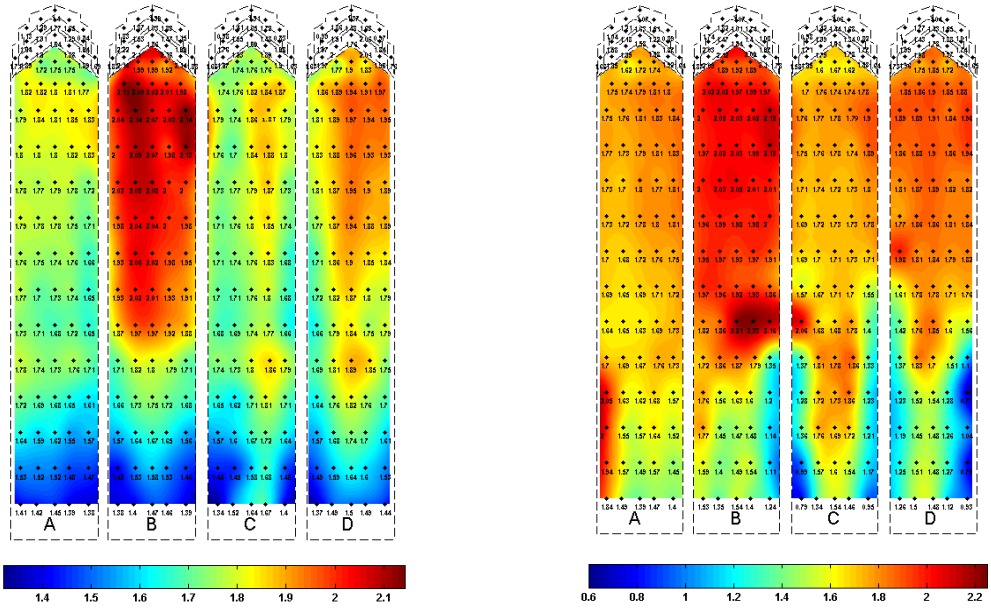

(a) Single case (b) Interference case

Fig. 5 The maximum wind pressure coefficient distribution of the main tower surface at different wind azimuth

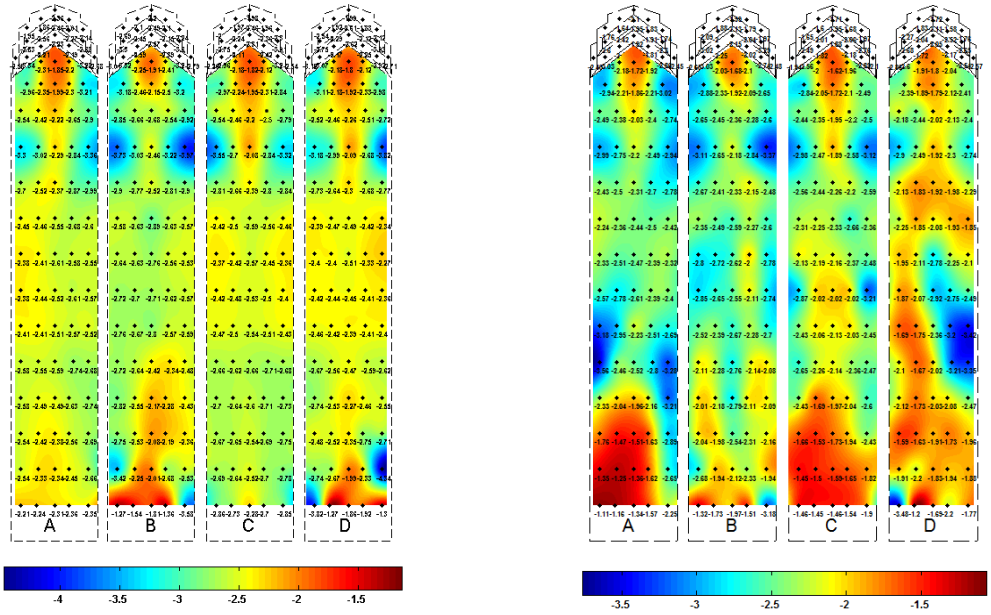

(a) Single case (b) Interference case

Fig. 6 The minimum wind pressure coefficient distribution of the main tower surface at different wind azimuth

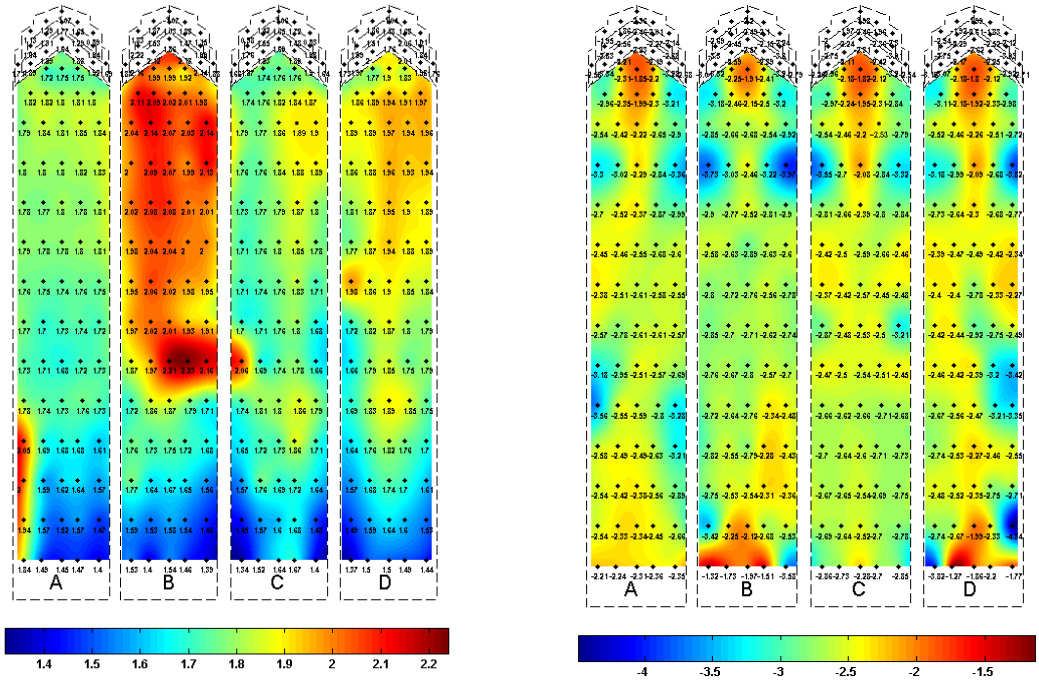

(a) Maximum value (b） Minimum value

Fig. 7 The envelope diagram of pressure coefficients for the main tower under different cases and wind azimuths

Table 2 The top 10 extreme wind pressure coefficients of the main tower under all wind azimuth

Tap. No	$C_{pi,\max}^{p}$	$W_{ki,\max}^{p}$	Tap. No	$C_{pi,\min}^{p}$	$W_{ki,\min}^{p}$
B59	4.46	2.23	D80	-8.69	-4.34
B10	4.44	2.22	B35	-7.95	-3.97
B58	4.41	2.21	D35	-7.64	-3.82
B15	4.33	2.16	D81	-7.63	-3.82
B60	4.32	2.16	B31	-7.46	-3.73
B27	4.28	2.14	B11	-7.20	-3.60
B30	4.27	2.14	B85	-7.17	-3.58
B16	4.27	2.14	A61	-7.11	-3.56
B13	4.27	2.13	C31	-7.09	-3.55
B35	4.26	2.13	B76	-6.85	-3.42

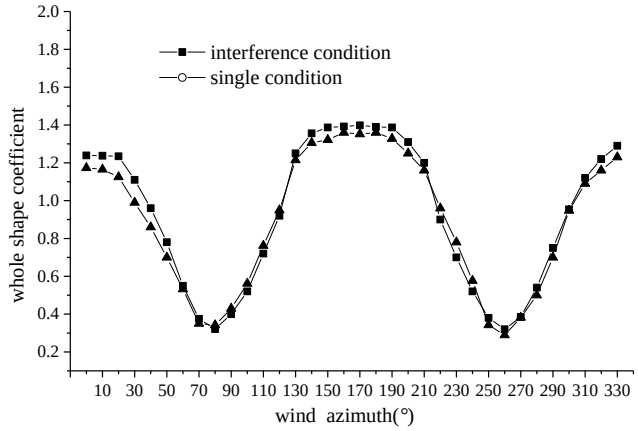

(a) Downwind (*X*-axis) direction

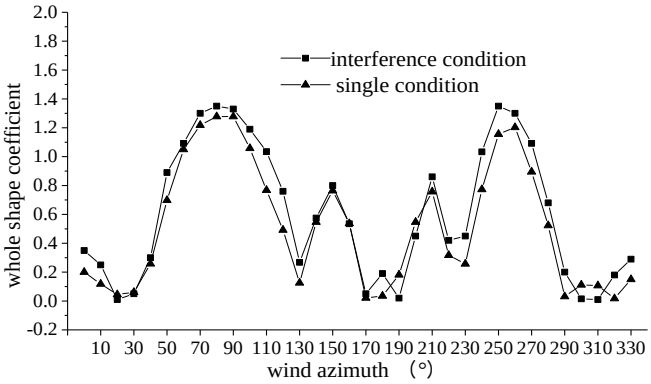

(b) Across-wind (*Y*-axis) direction

Fig. 8 The whole shape coefficients of the main building with different wind azimuth

are similar and homogeneous, and the minimum wind pressure coefficients under single condition are slightly less than the extreme values under interference condition.

(3) The extreme distribution of wind pressure coefficients shows that the sub-towers and surrounding buildings have some favorable blocking effects on surface wind loads of main tower structure of three-tower connected tall building. And for the convenience of selecting wind pressures of retaining structures, Table 2 presents the extreme wind pressure coefficients and the corresponding measuring point numbers.

The whole shape coefficients in two major axis directions under single and interference conditions are shown in Fig. 8. It can be found that the whole shape coefficients distribution in *X*-axis and *Y*-axis directions changes significantly with the wind azimuth, the whole shape coefficient in *X*-axis direction under interference condition reaches maximum 1.36 at 0° wind azimuth, and the whole shape coefficient in *Y*-axis direction under single condition reaches maximum 1.38 at 270° wind azimuth. The results show that the interference effect will reduce the whole wind load of the main tower structure, and the extreme whole shape coefficients under different conditions are greater than the whole shape coefficient 1.3 given by the Chinese loads specification (GB50009-2012 2012), which should attract attention for the wind-resistant design of such three-tower connected tall building.

4.4 Wind-induced responses characteristics

Based on the wind tunnel test and refined calculating method proposed in this paper, the maximum acceleration responses of main tower top under single and interference conditions with different wind azimuths, Fig. 9 shows the acceleration responses in *X*-axis and *Y*-axis directions under the wind loads of 10-year return period. It can be found from the figures that:

(1) The acceleration responses in *X*-axis and *Y*-axis directions under single condition respectively reach maximum values 0.127 m/s^2 and 0.112 m/s^2 at 280° and 0° wind azimuths, and the total acceleration response 0.123 m/s^2 peaks in wind azimuth 280°, the maximum acceleration response meets the comfort limit 0.15 m/s^2 for high-rise buildings.

(2) For the interference condition, when the wind azimuth changes between 0° to 360°, the

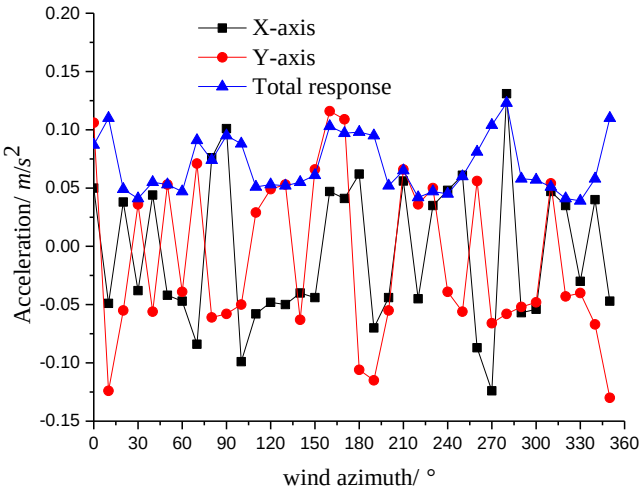

(a) Single condition

Fig. 9 The acceleration responses of main tower top with different wind azimuths

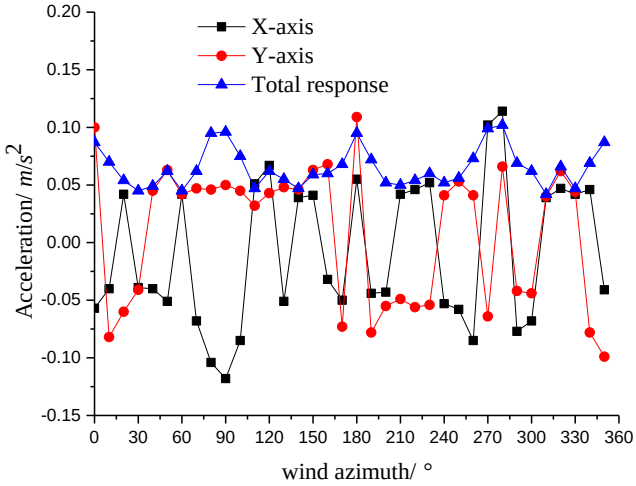

(b) Interference condition

Fig. 9 Continued

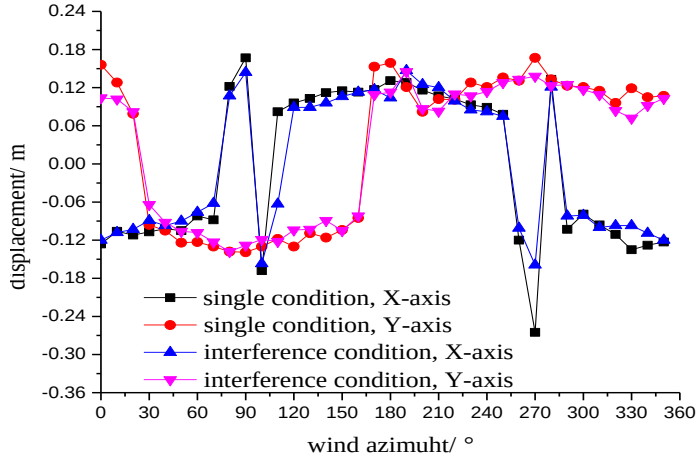

Fig. 10 The displacement responses of main tower top under different wind azimuths

acceleration responses in *X*-axis and *Y*-axis directions respectively reach maximum values 0.108 m/s^2 and 0.107 m/s^2 in 280° and 160° wind azimuths, and total acceleration response 0.102m/s^2 peaks in wind azimuth 280°, the extreme acceleration responses all appear in the across-wind direction, which indicates that the acceleration response in across-wind direction induced by vortex shedding phenomenon is stronger than acceleration response in along-wind direction induced by turbulent wind, and the vortex shedding phenomenon is approximate strongest when wind is perpendicular to the building surface.

Fig. 10 presents the displacement responses of main tower top under single and interference conditions with different wind azimuths. It can be found from the figures that displacement responses in single condition mostly are greater than the responses in interference condition, especially within the scope of 0° to 90° and 270° to 360° wind azimuth, where the main tower is

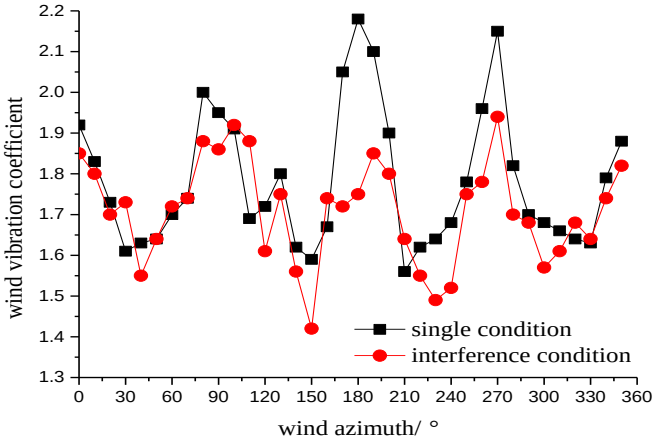

Fig. 11 The wind vibration coefficients of main tower top under different wind azimuths

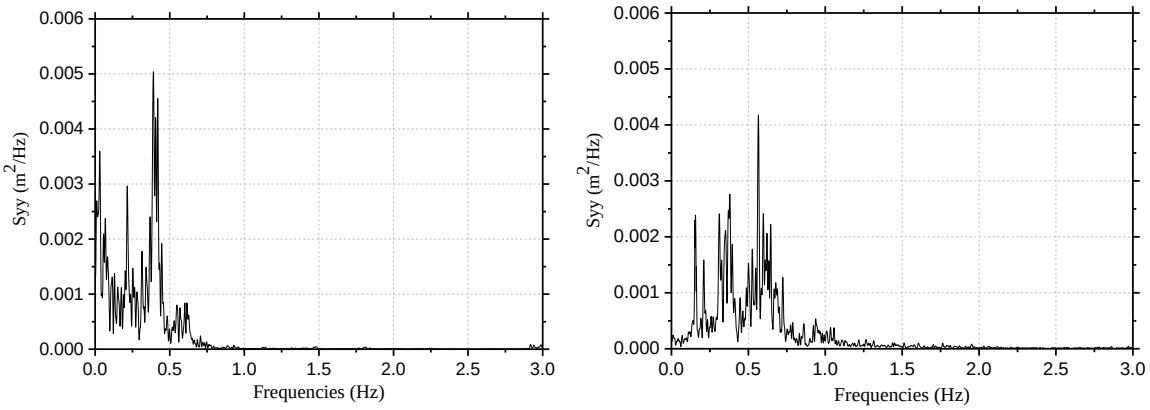

(a) single condition (b) interference condition

Fig. 12 Power spectrum density function of dynamic displacement on structural top in 0° wind direction

just located the downstream wake of sub-towers and surrounding buildings, the result indicates that the interference effect will reduce the displacement response of the main tower top. When the wind azimuth changes from 0° to 360°, the maximum displacement response under single condition appears in the wind azimuth 280°, and the extreme value is 0.275 m in *X*-axis direction, meanwhile, the displacement response reaches maximum value 0.162 m in *Y*-axis direction in 0° wind azimuth.

The wind vibration coefficient is a key parameter in the structural wind-resistant design. Fig. 11 gives the wind vibration coefficients of main tower top under different wind azimuth. The main conclusions can be drawn as follow:

The wind vibration coefficients under single and interference conditions have different change rules with wind azimuths, the maximum wind vibration coefficient 2.18 in single condition peaks at 180° wind azimuth, with the increase of wind azimuth, there is a second extreme value 2.14 at 280° wind azimuth. Compared with the results in single condition, the wind vibration coefficients in interference condition are generally smaller, and the maximum value is only 1.95 in 280° wind

azimuth.

Fig. 12 presents the power spectrum density function of dynamic displacement in *X*-axis direction on main tower top in 0° wind azimuth, it can be found that the resonant response component plays a comparatively important role in the total fluctuating response, the contributions from the modes whose frequencies are higher than 2.0 Hz to the responses are mainly quasi-static responses. The interference effect from sub-towers and surrounding buildings could induce the more resonant modes, but the RMS of total dynamic displacement in interference condition is less than the that in single condition.

In order to discuss the coupled effects and to verify the precision of the present method for computation of wind-induced displacement responses on tower top, the full-mode CQC method, SRSS method, IWL method, tri-component method and the present method are used to calculate the RMS of fluctuating responses with and without interference conditions. TCM-1 is the tri-component method, which omits the coupled effect of resonant modes, while TCM-2 is the tri-component method, which considers the coupled effect of resonant modes. However, the two methods cannot consider the coupled component between background and resonant responses.

From Table 3, it can be found that the response values obtained by SRSS and IWL methods obviously deviate from the precise values, with a maximum error of 19.3% under single condition. The differences between the calculation results of TCM-1 and TCM-2 indicate that the coupled effect between resonant modes should be taken into account. The values obtained by the present method are very close to the exact results. The biggest difference from the other methods is that the present method considers the coupled effect between background and resonant responses, and coupled effects between the resonant modes, which introduces a new thought for analyzing characteristics of wind-induced responses for this three-tower connected buildings.

4.5 The basal and floor ESWLs

According to the analysis results of whole wind loads and displacement responses of tower top, the four wind azimuths 0°, 90°, 180° and 280° are selected as the unfavorable working conditions for the structural floor ESWLs, and the calculating damping ratios respectively are 2.5%, 2.0% and 1.5%, basic wind pressures are respectively 50-year return period and 20-year return period. Fig. 13 shows the structural floor ESWLs in *X*-axis and *Y*-axis direction under different calculating conditions, and the target load effect is the structural top displacement. It can be found in the following conclusions:

(1) For the structural floor ESWLs in *X*-axis direction with different wind azimuths, the ESWLs in single condition are obviously greater than the results in interference condition, and the ESWLs in 0° and 180° wind azimuths can envelope the results in other wind azimuth. The ESWLs in *Y*-axis direction under single condition is much greater than the ESWLs in interference condition under 110 m height, but above the 110 m height the ESWLs in single

Table 3 RMS of wind-induced responses on tower top by different calculation methods (unit: m)

Condition	Full-mode CQC (exact solution)	SRSS	IWL	TCM-1	TCM-2	The present method
Single	0.31	0.28	0.25	0.28	0.30	0.30
Interference condition	0.36	0.32	0.29	0.31	0.33	0.35

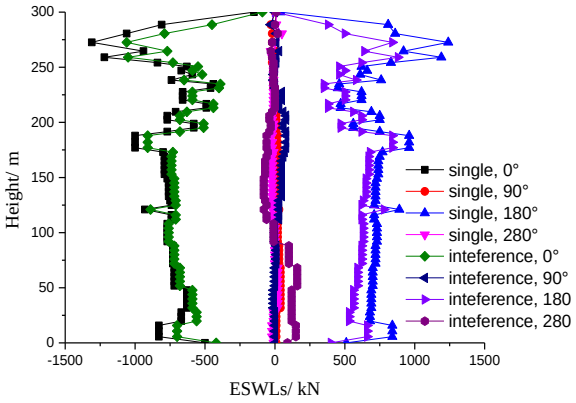

(a) 50-year return period+2.5% damping ratio, *X*-axis direction

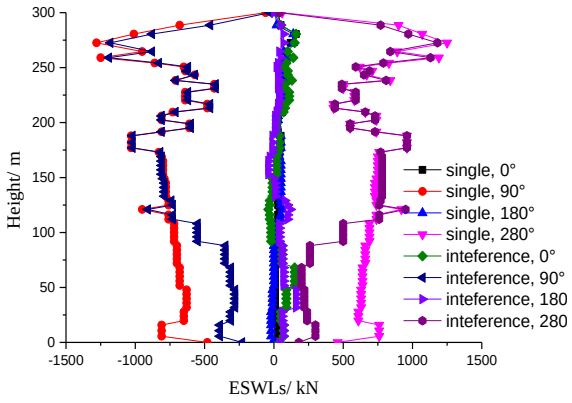

(b) 50-year return period+2.5% damping ratio, *Y*-axis direction

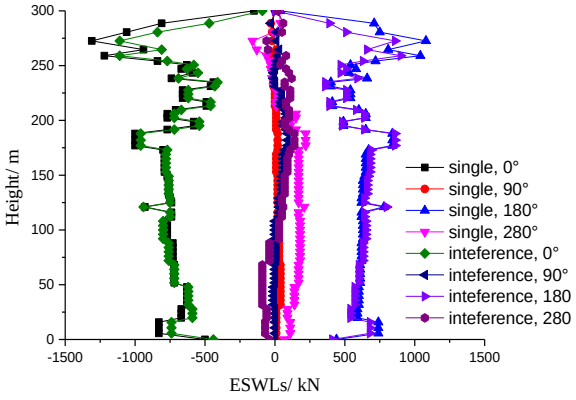

(c) 50-year return period+2% damping ratio, *X*-axis direction

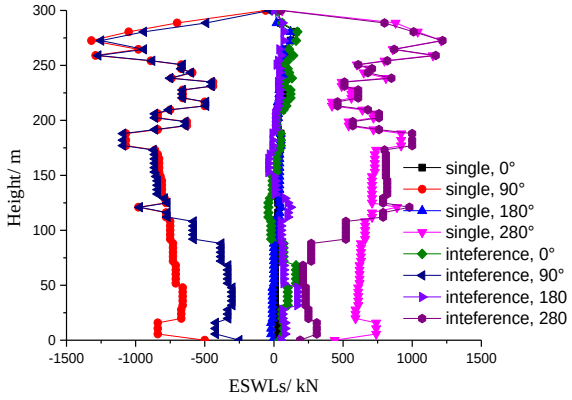

(d) 50-year return period+2% damping ratio, *Y*-axis direction

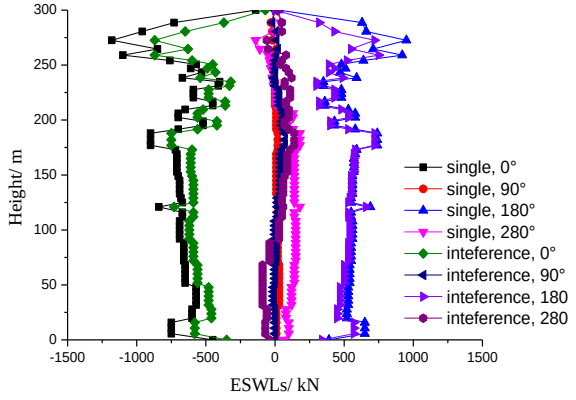

(e) 20-year return period+1.5% damping ratio, *X*-axis direction

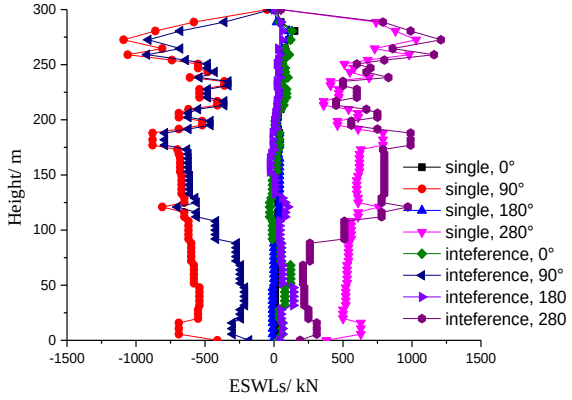

(f) 20-year return period+1.5% damping ratio, *Y*-axis direction

Fig. 13 The floor ESWLs of main tower structure with different calculating cases

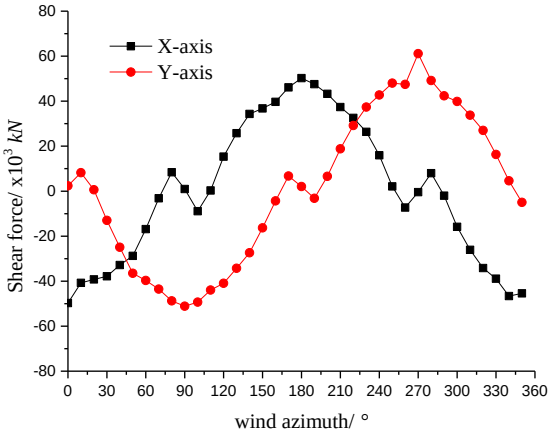

(a) basal shear forces under single condition

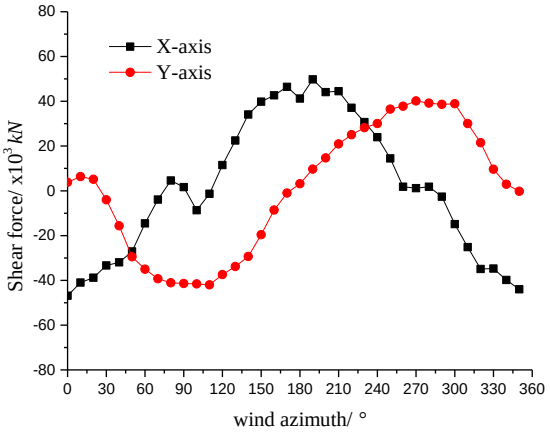

(b) basal shear forces under interference condition

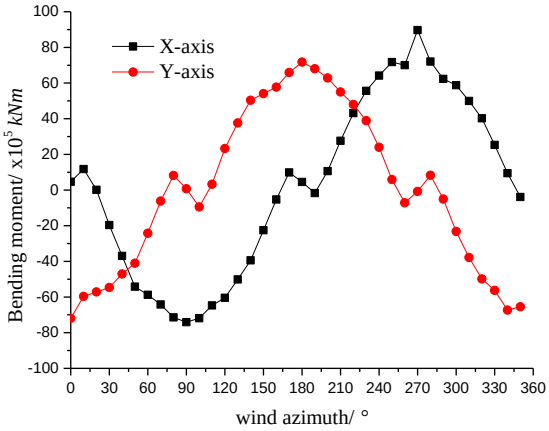

(c) basal bending moment under single condition

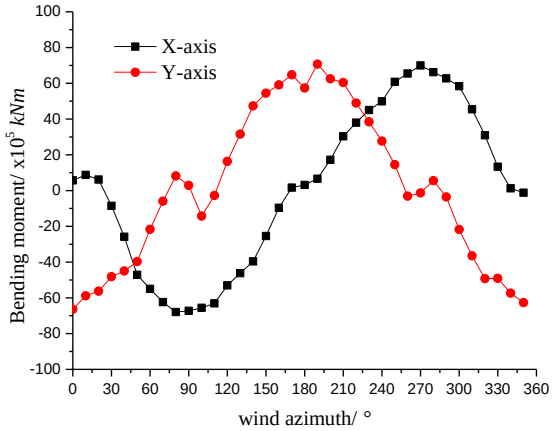

(d) basal bending moment under interference

Fig. 14 The basal ESWLs of main tower under different calculating cases

condition are close to the ESWLs in interference condition, and the ESWLs in 90° and 280° wind azimuths can envelope the results in other wind azimuth.

(2) With the increase of structural height, the ESWLs are amplified gradually, when up to 160m height (closed to the sub-tower height 156 m), the ESWLs will appear strong jumping phenomenon, it shows that there are strong upward flow pressures above the 160 m of the main tower, which make the drastic fluctuations of ESWLs in *X*-axis and *Y*-axis directions. This phenomenon is very different from the ordinary isolated tall building, which should cause enough attention in the wind-resistant design.

In order to analyze the interference effect on whole wind loads for main tower structure, the equivalent basal shear forces and bending moments in *X*-axis and *Y*-axis directions based on 50-year return period and 2.5% damping ratio are shown in Fig. 14. It can be found that the basal force distributions under single and interference conditions are similar, but the basal shear forces under single condition are significantly greater than the results under interference condition. The maximum basal shear forces in *X*-axis and *Y*-axis directions under single condition respectively appear in 180° and 270° wind azimuths, and the maximum basal shear forces in *X*-axis and *Y*-axis

Table 4 The peak basal ESWLs of main tower with different calculating cases

Case number	Case description	V_x (MN)	M_y (MNm)	V_y (MN)	M_x (MNm)
Case 1	(1.1x) 50-year return period + 2.5% damping ratio	49.787	7074.667	42.018	6999.673
Case 2	50-year return period + 2% damping ratio	46.654	6485.365	41.244	6845.691
Case 3	20-year return period + 1.5% damping ratio	42.295	6010.066	40.142	6783.660
Error analysis	Case2 / case1	93.7%	91.6%	98.1%	97.8%
	Case3 / case1	84.9%	84.9%	95.3%	96.9%

directions under interference condition respectively appear in 190° and 280° wind azimuths, which respectively have 5% and 28% smaller than the results in single condition. The maximum bending moments around *X*-axis under single and interference conditions both peak in 270° wind azimuths, and the maximum bending moments around *Y*-axis under single and interference conditions respectively peak in 190° and 280° wind azimuths, the bending moments in interference condition respectively have 4% and 21% greater than the results in single condition.

In order to discuss the errors with different design standards, Table 4 presents the maximum basal forces in *X*-axis and *Y*-axis directions under single and interference conditions with different calculating parameters shown in the second column in Table 4. It can be found from the table that the basal shear forces and bending moments under calculating case 1 is greatest, which can envelop the calculating results under case 2 and 3, furthermore, the calculating results under case 2 are more close to calculating results under case 1, the calculating results under case 3 are smallest with the maximum error 15.1% for the shear force in *X*-axis direction. Therefore, the calculating parameters of case 1, e.g., 50-year return period (1.1 times), 2.5% damping ratio, are suitable for wind-resistant design of such three-tower connected tall building.

5. Conclusions

The wind loads, wind-induced displacement, wind vibration coefficients, acceleration responses, basal and floor ESWLs for the three-tower connected tall building have been studied based on measured synchronous surface pressures in a wind tunnel. The main results of this study present some new results that help to better understand and quantify wind-induced response of such three-tower connected tall building.

- The extreme wind pressures and whole shape coefficients in single condition are significant greater than the results in interference condition, and the interference buildings have more influence on the maximum wind pressures than the minimum wind pressures. The maximum wind pressures with different wind azimuths are mostly located in the upper area of surface *B*, however, the minimum wind pressures in four surfaces are similar and homogeneous. The structural whole shape coefficient reaches maximum value 1.38 in *Y*-axis direction when the wind is perpendicular to the *X*-axis (270° wind azimuth), which is greater than the whole shape coefficient 1.3 given by the Chinese loads specification.
- The interference effect from sub-towers and surrounding buildings significantly reduce the peak values of acceleration responses, displacement responses and wind vibration coefficients

on main tower top. The maximum acceleration response of 0.127 m/s^2 is found in *X*-axis direction at wind azimuth 280° under single condition, the maximum displacement response of 0.275 m is also found in *X*-axis direction at wind azimuth 280° under single condition, and the maximum wind vibration coefficient of 2.18 is found in *Y*-axis direction at 180° wind azimuth. It is found that the peak responses all appear in the across-wind direction, which indicates that the dynamic wind effects in across-wind direction induced by vortex shedding phenomenon is stronger than acceleration response in along-wind direction induced by turbulent wind, and the vortex shedding phenomenon is approximate strongest when wind is perpendicular to the building surface.

• The floor ESWLs in unfavorable wind azimuths under single condition are slightly greater than the results under interference condition, especially under 110 m height. With the increase of structural height, the floor ESWLs are amplified gradually, when up to 160 m height (closed to the sub-tower height 156 m), the ESWLs will appear strong jumping phenomenon, which indicates that there are strong upward flow pressures above the 160 m of the main tower, which make the drastic fluctuations of ESWLs in *X*-axis and *Y*-axis directions. This phenomenon is very different from the ordinary isolated tall building, which should cause enough attention in the wind-resistant design.

• The maximum basal shear forces and bending moments in *X*-axis and *Y*-axis directions are mostly found in wind azimuths 190° and 280°, and the basal forces in single condition have approximate 12% smaller than those in interference condition. The calculating parameters of case 1, e.g., 50-year return period (1.1 times), 2.5% damping ratio, are suitable for wind-resistant design of such three-tower connected tall building.

Acknowledgments

This project is jointly supported by National Natural Science Foundation (50978203, 51208254) and Jiangsu Province Natural Science Foundation (BK2012390) and China Postdoctoral Science Foundation (2013M530255), which are gratefully acknowledged.

Reference

Bailey P.A. and Kwok K.C.S. (1985), "Interference excitation of twin tall buildings", *Wind Eng. Ind. Aerodyn.*, **21**, 323-338.

Chen, X. and Kareem, A. (2005), "Dynamic wind effects on buildings with threedimensional coupled modes: Application of high frequency force balance measurements", *Eng. Mech.*, **131**(11), 1115-25.

Davenport, A.G. (1967), "Gust loading factors", *Struct. Div.*, ASCE, **93**(3), 11-34.

GB50009-2012 (2012), Load code for the design of building structures, The Ministry of Structure of the People's Republic of China, Beijing. (in Chinese)

Holmes, J.D. (2002), "Effective static load distributions in wind engineering", *Wind Eng. Ind. Aerodyn.*, **90**, 91-109.

Huang, G.Q. and Chen, X.Z. (2007), "Wind load effects and equivalent static wind loads of tall buildings based on synchronous pressure measurements", *Eng. Struct.*, **29**, 2641-2653

Kareem, A. (1981), "Wind-excited response of buildings in higher modes", *Struct. Div.*, ASCE, **107**(4), 701-706.

Kareem, A. and Zhou, Y. (2003), "Gust loading factor: Past, present, and future", *Wind Eng. Ind. Aerodyn.*,

91(12-15), 1301-28.
Kasperski, M. (1992), "Extreme wind load distributions for linear and nonlinear design", *Eng. Struct.*, **14**, 27-34.
Kasperski, M. and Niemann, H.J. (1992), "The LRC (load-response correlation) method: a general method of estimating unfavorable wind load distributions for linear and nonlinear structural behavior", *Wind Eng. Ind. Aerodyn.*, **43**, 1753-1763.
Katsumura, A., Tamura, Y. and Nakamura, O. (2007), "Universal wind load distribution simultaneously reproducing largest load effects in all subject members on large-span cantilevered roof", *Wind Eng. Ind. Aerodyn.*, **95**, 1145-1165.
Khanduri, A.C. (1998), "Stathopoulos T, Bedard C.Wind-induced interference effects on buildings-A review of the state-of-the-art", *Eng. Struct.*, **20**(7), 617-630.
Kim, W., Tamura, Y. and Yoshida, A. (2011), "Interference effects on local peak pressures between two buildings", *Wind Eng. Ind. Aerodyn.*, **99**, 584-600
Lam, K.M., Leung, M.Y.H. and Zhao, J.G. (2008), "Interference effects on wind loading of a row of closely spaced tall buildings", *Wind Eng. Ind. Aerodyn.*, **96**, 562-583
Li, H. and Sumner, D. (2009), "Vortex shedding from two finite circular cylinders in a staggered configuration", *Fluid. Struct.*, **25**, 479-505.
Liang, S.G., Zou, L.H., Wang, D.H. and Huang, G.Q. (2014), "Analysis of three dimensional equivalent static wind loads of symmetric high-rise buildings based on wind tunnel tests", *Wind Struct.*, **19**(5), 563-583.
Lim, J., Bienkiewicz, B. and Richards, E. (2011), "Modeling of structural coupling for assessment of modal properties of twin tall buildings with a skybridge", *J. Wind Eng. Indus. Aerodyn.*, **99**(5), 615-623.
Simiu, E. (1976), "Equivalent static wind loads for tall building design", *Struct. Div.*, ASCE, **102**(4), 719-37.
Simiu, E. and Scanlan, R.H. (1996), *Wind effects on structures: Fundamentals and applications to design*, 3rd Edition, New York: John Wiley & Sons, Inc.
Solari, G. and Kareem, A. (1998), "On the formulation of ASCE 7-95 gust effect factor", *Wind Eng. Ind. Aerodyn.*, **77-78**, 673-84.
Song, J. and Tse, K.T. (2014), "Dynamic characteristics of wind-excited linked twin buildings based on a 3-dimensional analytical model", *Eng. Struct.*, **79**(79), 169-181.
Song, J., Tse, K.T., Tamura, Y. and Kareem, A. (2016), "Aerodynamics of closely spaced buildings: With application to linked buildings", *J. Wind Eng. Indus. Aerodyn.*, **149**, 1-16.
Tanaka, H., Tamura, Y., Ohtake, K., Nakai, M. and Kim, Y.C. (2012), "Experimental investigation of aerodynamic forces and wind pressures acting on tall buildings with various unconventional configurations", *J. Wind Eng. Indus. Aerodyn.*, **107-108**(8), 179-191.
Tse, K.T. and Song, J. (2015), "Modal analysis of a linked cantilever flexible building system", *J. Struct. Eng.*, **141**. 0415008.
Xie, Z. and Gu, M. (2004), "Mean interference effects among tall buildings", *Eng. Struct.*, **26**, 1173-1183.
Xie, Z.N. and Gu, M. (2007), "Simplified formulas for evaluation of wind-induced interference effects among three tall building", *Wind Eng. Ind. Aerodyn.*, **95**, 31-52.
Zhao, J.G. and Lam, K.M. (2008), "Interference effects in a group of tall buildings closely arranged in an L- or T- shape pattern", *Wind Struct.*, **11**(1), 1-18
Zhou, X., Huang, P., Gu, M. and Mi, F. (2011), "Wind loads and responses of two neighboring dry coal sheds", *Adv. Struct. Eng.*, **14**(2), 207-221.
Zhou, Y. and Kareem, A. (2001), "Gust loading factor: New model", *Struct. Eng.*, **127**(2), 168-175.